

# Theory of Energy Transfer in Organic Nanocrystals

Rocío Sáez-Blázquez, Johannes Feist, Francisco J. García-Vidal,\*  
and Antonio I. Fernández-Domínguez\*

Recent experiments have shown that highly efficient energy transfer can take place in organic nanocrystals at extremely low acceptor densities. This striking phenomenon has been ascribed to the formation of exciton polaritons thanks to the photon confinement provided by the crystal itself. An alternative theoretical model that accurately reproduces fluorescence lifetime and spectrum measurements in these systems without such an assumption is proposed. The approach treats molecule–photon interactions in the weak-coupling regime, and describes the donor and acceptor population dynamics by means of rate equations with parameters extracted from electromagnetic simulations. The physical insight and predictive value of this model also enables the authors to propose nanocrystal configurations in which acceptor emission dominates the fluorescence spectrum at densities orders of magnitude lower than the experimental ones.

of difluoroboron chromophores, in which aggregation-induced emission did not occur<sup>[16]</sup> and with relative acceptor densities of the order of  $10^{-3}$ . More surprisingly, the measured fluorescence spectra showed fingerprints of energy transfer in experimental samples with densities as small as  $5 \times 10^{-5}$ .

Concurrently with these advances in artificial light-harvesting, research interests have also focused on polaritons as a means to enhance energy transfer. Experimental<sup>[17–19]</sup> and theoretical<sup>[20–22]</sup> reports have shown that the coherent and delocalized character of these hybrid light-matter states makes it possible to increase the spatial range and temporal rate of energy transfer processes. Strong coupling


## 1. Introduction

Artificial light-harvesting systems have received much attention lately. They are inspired by the pigment-protein antenna complexes of natural photosynthesis, which convey the solar energy into the reaction centers with efficiencies approaching 100%.<sup>[1,2]</sup> Mimicking bacterial and plant photosynthetic units,<sup>[3]</sup> which present a large number of antennas per reaction center,<sup>[4]</sup> these artificial structures aim for high transfer efficiencies at low acceptor/donor ratios.<sup>[5]</sup> Several experimental configurations have been explored in this context, including dendrimers and multiporphyrin arrays,<sup>[6,7]</sup> multilayer polymer films,<sup>[8,9]</sup> and other heterostructures<sup>[6,10]</sup> and supramolecular compounds.<sup>[11–14]</sup> In a recent experiment carried out by Chen and co-workers,<sup>[15]</sup> 95% transfer efficiency was reported in nanocrystals

between photons and molecular excitons has been also investigated in photosynthetic complexes.<sup>[23–25]</sup> Very recently, it has been argued<sup>[26]</sup> that the formation of polaritons is the underlying mechanism behind the efficient energy transfer reported in organic nanocrystals at extremely low acceptor densities. In this theory, the nanocrystal itself would act as an optical cavity, providing the photon confinement required for strong coupling.

Here, we present a theoretical model for the process of energy transfer in organic nanocrystals. Our approach depicts photon–molecule interactions in the weak-coupling regime, and accounts for the population dynamics of donor and acceptor ensembles by means of coupled rate equations. These are parameterized by radiative and nonradiative Purcell factor simulations based on numerical solutions of Maxwell's equations. Without the need of any fitting procedure, our model accurately describes the experimental results in ref. [15]. Fluorescence spectra and donor lifetime measurements are reproduced systematically by means of steady-state and transient calculations for acceptor/donor ratios two orders of magnitude apart. Our findings reveal that the combination of the short-range Förster mechanism<sup>[27,28]</sup> and the inherently large donor densities in organic nanocrystals<sup>[29]</sup> makes energy transfer highly efficient even in conditions of extremely low acceptor concentrations. Contrary to what has been proposed in ref. [26], we show that there is no significant photon confinement in these systems, which prevents the formation of exciton polaritons. Finally, we employ our model to investigate if the process of energy transfer could be modified by introducing the samples in an optical cavity. We find that while its efficiency cannot be tailored this way, it is possible to design crystal-cavity configurations in which acceptor emission governs the fluorescence spectrum at relative concentrations as small as  $10^{-5}$ .

R. Sáez-Blázquez, Dr. J. Feist, Prof. F. J. García-Vidal,  
Dr. A. I. Fernández-Domínguez  
Departamento de Física Teórica de la Materia Condensada and  
Condensed Matter Physics Center (IFIMAC)  
Universidad Autónoma de Madrid  
E-28049, Madrid, Spain  
E-mail: f.j.garcia@uam.es; a.fernandez-dominguez@uam.es  
Prof. F. J. García-Vidal  
Donostia International Physics Center (DIPC)  
Donostia/San Sebastián E-20018, Spain

 The ORCID identification number(s) for the author(s) of this article can be found under <https://doi.org/10.1002/adom.202001447>.

© 2020 The Authors. Published by Wiley-VCH GmbH. This is an open access article under the terms of the Creative Commons Attribution-NonCommercial License, which permits use, distribution and reproduction in any medium, provided the original work is properly cited and is not used for commercial purposes.

DOI: 10.1002/adom.202001447

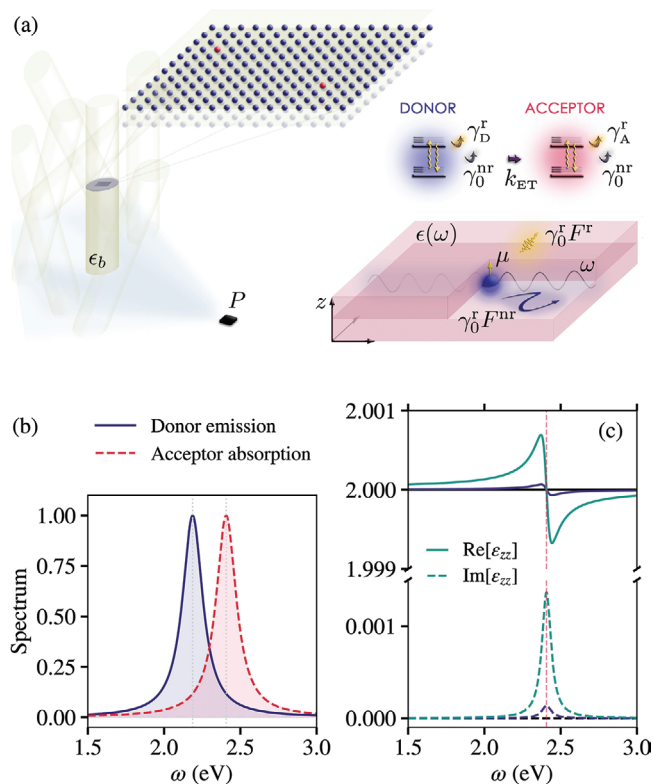


**Figure 1.** a) Scheme of the organic nanocrystal system, with the relevant parameters characterizing our modeling. b) Donor emission (continuous blue line) and acceptor absorption (dashed red line) spectra. c) Real (continuous lines) and imaginary (dashed lines) parts of the  $zz$ -component of the permittivity for two different acceptor densities:  $n = 10^{-5} \text{ nm}^{-3}$  (blue) and  $n = 10^{-4} \text{ nm}^{-3}$  (green).

## 2. Results and Discussion

The first ingredient in our approach is the introduction of the two-level system model for the donor and acceptor molecules. Both are sketched in **Figure 1a** in blue and red colors, respectively. The samples in ref. [15] were composed of  $\text{BF}_2\text{bcz}$  (donors) nanocrystals presenting different (controlled) densities of  $\text{BF}_2\text{cna}$  (acceptors) impurities in their structure. Mimicking the experimental data, we set their emission frequencies to  $\omega_D^{\text{em}} = 2.187 \text{ eV}$  and  $\omega_A^{\text{em}} = 2.013 \text{ eV}$ , respectively. The acceptor absorption is centered at  $\omega_A^{\text{ab}} = 2.407 \text{ eV}$ , overlapping significantly with the donor emission, see **Figure 1b**. All the spectra are modeled as Lorentzian-like profiles of the form

$$S_i^o(\omega) = \frac{1}{\pi} \frac{\sigma}{(\omega - \omega_i^o)^2 + \sigma^2} \quad (1)$$

where  $i = D, A$ , and  $o = \text{em}, \text{ab}$  stands for emission or absorption, respectively. We set  $\sigma = 0.08 \text{ eV}$  to account for the width of the measured spectra. Note that, for simplicity, we do not consider here  $\text{BF}_2\text{dan}$  acceptor chromophores, which were also studied in the experiment yielding similar results as  $\text{BF}_2\text{cna}$  samples.

Our description of the energy transfer mechanism through electromagnetic simulations treats donor molecules as independent dipolar point sources. This is a valid assumption for our target nanocrystal samples, but would fail for systems in which large dipole–dipole interactions take place, giving rise to phenomena such as aggregation-induced emission or quenching.<sup>[16]</sup> The molecule orientation is set by the crystal-line structure (we assume they point along the  $z$ -direction). The ensemble of acceptor molecules embedded in the crystal structure is modeled through an effective dielectric function. Assuming that acceptor and donor chromophores have the same orientation, the nanocrystal diagonal permittivity has the form  $\epsilon(\omega) = [\epsilon_b, \epsilon_b, \epsilon_{zz}(\omega)]$ . The lossless bare crystal permittivity is set to  $\epsilon_b = 2$ <sup>[26]</sup> and

$$\epsilon_{zz}(\omega) = \epsilon_b \frac{1 + 2n\alpha(\omega)/(3\epsilon_0)}{1 - n\alpha(\omega)/(3\epsilon_0)} \quad (2)$$

is given by the Clausius–Mossotti relation<sup>[30]</sup> where  $n$  is the number of acceptor molecules per unit volume and  $\epsilon_0$  is the vacuum permittivity. The polarizability of a single acceptor chromophores reads<sup>[31]</sup>

$$\alpha(\omega) = \frac{\mu^2}{\hbar} \frac{2\omega_A^{\text{ab}}}{(\omega_A^{\text{ab}})^2 - (\omega + i\sigma)^2} \quad (3)$$

where  $\mu$  is the molecular transition dipole moment.

Difluoroboron chromophores present a fluorescence lifetime  $\tau = 5.5 \text{ ns}$  and a quantum yield  $\Phi = 0.4$ .<sup>[32]</sup> Using these values, we can compute their radiative and nonradiative decay rates,  $\gamma_D^r = \Phi/\tau$  and  $\gamma_D^{\text{nr}} = (1 - \Phi)/\tau$ , as well as the acceptor dipole moment in Equation (3),  $\mu = \sqrt{3\pi c^3 \epsilon_0 \gamma_D^r / (\omega_A^{\text{em}})^3} = 0.12 \text{ e} \cdot \text{nm}$ .<sup>[33]</sup> **Figure 1c** plots the real (continuous lines) and imaginary (dashed lines) parts of the  $zz$ -component of the nanocrystal permittivity as a function of frequency for two different acceptor concentrations:  $n = 10^{-5} \text{ nm}^{-3}$  (blue) and  $n = 10^{-4} \text{ nm}^{-3}$  (green). We can observe that, as expected,  $\text{Im}\{\epsilon_{zz}(\omega)\}$  is governed by a maximum at  $\omega = \omega_A^{\text{ab}}$ , the center of the acceptor absorption band, marked with a vertical dashed red line. Note that the maximum absorption increases with the acceptor density  $n$ .

We use the effective medium permittivity in Equation (2) to compute the Purcell factor experienced by donor molecules in cylindrically-shaped nanocrystals. Their diameter and height are set to  $800 \text{ nm}$  and  $5 \mu\text{m}$ , respectively, in accordance with the dimensions of the experimental samples. By numerically solving Maxwell's equations using the finite element module of the commercial software COSMOL Multiphysics, we can compute the fraction of the power emitted by the donor molecules that is radiated into the far-field and absorbed by the acceptor chromophore ensemble. Normalizing to the power emitted in free-space, we can obtain the radiative and nonradiative Purcell factors,  $F^r$  and  $F^{\text{nr}}$ , respectively. We fix the donor density to  $1 \text{ nm}^{-3}$ , the inverse of the volume per molecule reported theoretically for  $\text{BF}_2\text{bcz}$  crystals.<sup>[29]</sup> This value is also in agreement with the interlayer distance reported experimentally. In order to link the nonradiative Purcell factor with the energy transfer rate in the systems, we exclude a cylindrical volume of  $3 \text{ nm}^3$  around the donor molecule in the calculation of  $F^{\text{nr}}$ . This way, we account for the fact that molecular

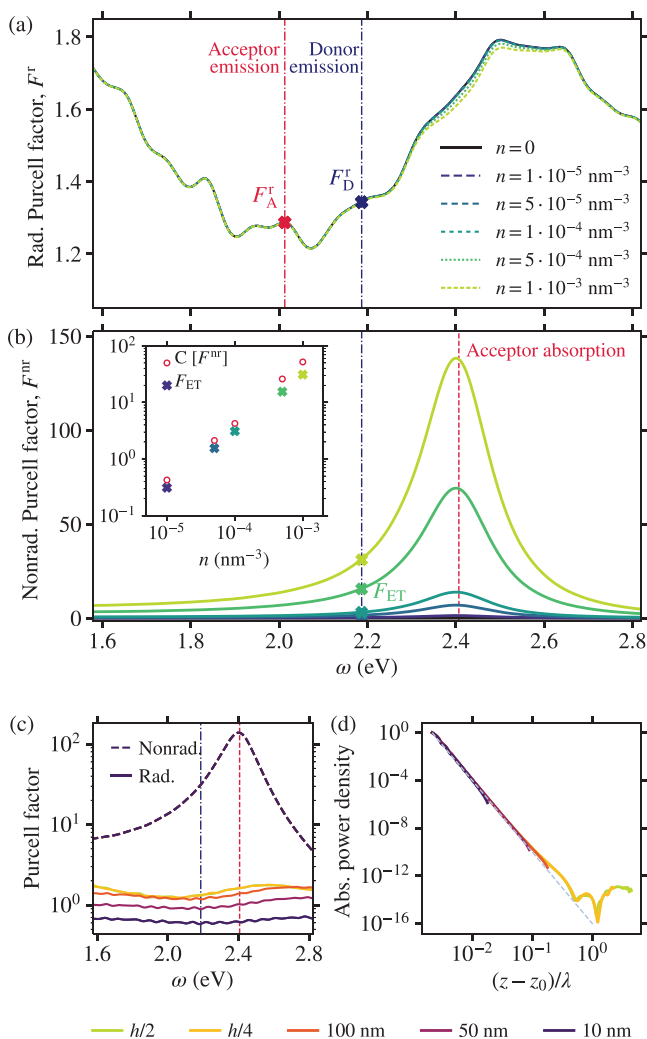


**Figure 2.** a) Radiative and b) nonradiative Purcell spectra for different values of the acceptor density  $n$ . Vertical dash-dotted lines indicate the donor (blue) and acceptor (red) emission frequencies, and the dashed red line marks the acceptor absorption frequency. The inset plots the normalized transfer rate versus the acceptor density  $n$  calculated as  $F^{nr}(\omega_D^{em})$  (crosses) and incorporating the whole donor emission band (circles). c) Radiative (solid lines) and nonradiative (dashed lines) Purcell spectra for different donor positions. d) Absorbed power density as a function of the distance from the donor,  $(z - z_0)$ , normalized to the donor emission wavelength  $\lambda = 2\pi c/\omega_D^{em}$ . The  $1/(z - z_0)^6$  dependence is rendered in gray dashed line.

excitons are delocalized among  $\approx 10$  chromophores in  $\text{BF}_2\text{bcz}$  crystals.<sup>[29]</sup>

Figure 2a,b show radiative and nonradiative Purcell spectra, respectively, for different acceptor densities  $n$ . In these calculations, we have considered a single donor chromophore placed in the center of the nanocrystal. We can observe that  $F^r$  hardly varies when increasing the acceptor concentration, and its value is always close to one. On the contrary,  $F^{nr}$  exhibits a peak centered at the acceptor absorption frequency that, following  $\text{Im}\{\epsilon_{zz}(\omega)\}$ , grows with increasing  $n$ . As we will show next, we can ascribe the normalized energy transfer rate to the nonradiative Purcell factor evaluated at the donor emission frequency,  $F_{ET} = F^{nr}(\omega_D^{em})$ . This magnitude

is plotted against acceptor density in the inset of Figure 2b with colored crosses. A more rigorous description of the transfer rate incorporating the whole donor emission band,<sup>[34]</sup>  $C[F^{nr}] = \int d\omega S_D^{em}(\omega) F^{nr}(\omega) \gamma_D^r(\omega) / \int d\omega S_D^{em}(\omega) \gamma_D^r(\omega)$ , with  $\gamma_D^r(\omega) = \mu^2 \omega^3 / 3\pi c^3 \epsilon_0$ ,<sup>[33]</sup> is rendered in red empty circles. We can observe the agreement between both sets of calculations, with slightly increasing discrepancies at larger  $n$ . These results enable us to use  $F_{ET} = F^{nr}(\omega_D^{em})$  in the following.

Figure 2c explores the dependence of the Purcell spectra on the position of the donor molecule,  $z_0$ . Five different distances from the nanocrystal top face and along the  $z$ -axis are considered.  $F^{nr}$  (dashed lines) overlaps for all positions, from the crystal center to only 10 nm below its boundary. This indicates that, as expected from the Förster mechanism,<sup>[27,28]</sup> each donor chromophore transfers energy to those acceptor molecules that located only a few nanometers away from it. The radiative Purcell factor (solid lines) depends slightly on the donor position, ranging from 0.6 to 2. This is a clear indication that a strong photon confinement does not take place in the system.

Figure 2d plots the normalized absorbed power density ( $F_{ET}$  per unit volume) as a function of the vertical distance from the donor position,  $(z - z_0)$ , for the five  $z_0$  values in panel (c). The gray dashed line renders the  $1/(z - z_0)^6$  law characteristic of the Förster mechanism. We can observe that the absorbed power density follows this trend for all  $z_0$ , presenting only small deviations at the structure boundaries. Importantly, we can infer that the proportional relationship between  $F_{ET}$  and  $n$  apparent in Figure 2c originates from the volume integration of this inverse sixth-power dependence on the distance of the absorbed power density.

We employ next our electromagnetic model to construct a description of the donor and acceptor population dynamics in terms of a system of rate equations. These must include the decay and pumping channels experienced by each chromophore ensemble. The radiative decay rates of donor and acceptor molecules within the nanocrystal are computed from the Purcell factors evaluated at the corresponding emission frequencies,  $\gamma_{D/A}^r = \gamma_D^r F^r(\omega_{D/A}^{em})$ . Similarly, as discussed above, the energy transfer rate at different acceptor densities is given by  $k_{ET} = \gamma_D^r F_{ET} = \gamma_D^r F^{nr}(\omega_D^{em})$ . The external excitation of the system is accounted for through a pumping rate,  $P$ , acting only on the donor molecules. Thus, we can write the rate equations as

$$\begin{aligned} \frac{dn_D(t)}{dt} &= P - \gamma_D^{nr} n_D(t) - \gamma_D^r n_D(t) - k_{ET} n_D(t) \\ \frac{dn_A(t)}{dt} &= k_{ET} n_D(t) - \gamma_A^{nr} n_A(t) - \gamma_A^r n_A(t) \end{aligned} \quad (4)$$

where  $n_D$  and  $n_A$  stand for the donor and acceptor populations, respectively. Notice that we have introduced an additional term in the equations above, which describes the nonradiative losses experienced by both chromophores due to their relatively low intrinsic quantum yield.

The steady-state solution to Equation (4) describes the continuous pumping of the donor molecules, in a similar way as in a fluorescence measurement. This is obtained by imposing  $dn_{D/A}(t)/dt = 0$ , which yields the following populations:

$$n_D^{ss} = \frac{P}{\gamma_D^{nr} + \gamma_D^r + k_{ET}}, \quad n_A^{ss} = \frac{k_{ET}}{\gamma_A^{nr} + \gamma_A^r} n_D^{ss} \quad (5)$$

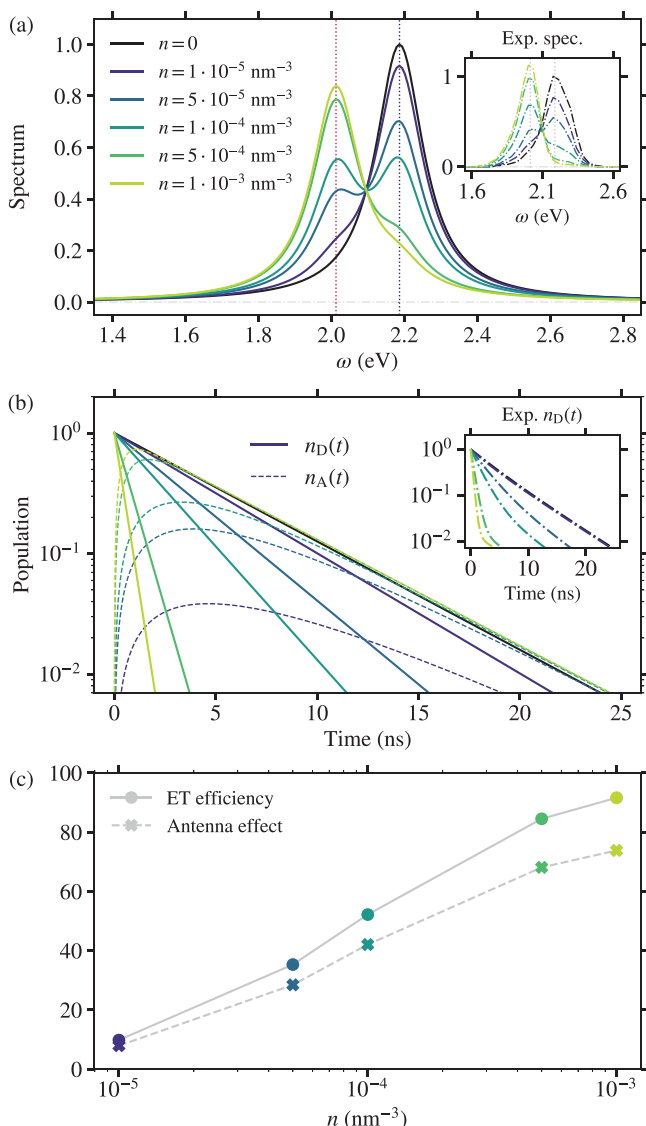


**Figure 3.** a) Theoretical fluorescence spectra for organic nanocrystals with different acceptor concentrations. Vertical dotted lines indicate the donor (blue) and acceptor (red) emission frequencies. b) Time evolution of the donor (continuous lines) and acceptor (dashed lines) populations for the same configurations as in panel (a). The insets in (a) and (b) display the experimental results in ref. [15]. c) Energy transfer efficiency (circles, continuous line) and antenna effect (crosses, dashed line) as a function of  $n$ .

Once the donor and acceptor steady-state populations are known, the fluorescence spectrum of the organic nanocrystal can be written as

$$S(\omega) = \gamma_D^r n_D^{ss} \omega_D^{em} S_D^{em}(\omega) + \gamma_A^r n_A^{ss} \omega_A^{em} S_A^{em}(\omega) \quad (6)$$

where  $S_D^{em}(\omega)$  and  $S_A^{em}(\omega)$  follow the Lorentzian profile given in Equation (1), and we have used that the power radiated by a single molecule scales as  $\gamma_D^r \omega_D^{em}$ .<sup>[33]</sup>

Figure 3a displays fluorescence spectra obtained from Equation (6) for different values of the acceptor density, ranging from  $n = 10^{-5} \text{ nm}^{-3}$  (purple) to  $n = 10^{-3} \text{ nm}^{-3}$  (yellow). Within

this window of acceptor/donor ratios ( $10^{-5}$  to  $10^{-3}$ ), the emission profile changes qualitatively. The spectrum in absence of acceptor molecules (black line) is shown as a reference (its maximum height is normalized to 1). The donor emission dominating this configuration decreases with larger acceptor density as a result of the energy transfer mechanism. Concurrently, fluorescence from acceptor molecules becomes more intense, and  $S(\omega)$  is fully governed by the acceptor Lorentzian at  $n = 10^{-3} \text{ nm}^{-3}$ . Importantly, the acceptor contribution to the spectrum is clearly visible at relative densities as low as  $5 \times 10^{-5}$ . This evolution of  $S(\omega)$  with acceptor concentration is the main result of this work, as it is in not only qualitative, but excellent quantitative agreement with the experimental spectra in ref. [15]. These are shown in the inset of Figure 3a using the same color code and normalization as in the theoretical predictions to facilitate the comparison. The predictive value of our model, which systematically reproduces the dependence of the spectrum on  $n$ , enables us to conclude that it captures all the relevant physical mechanisms playing a role in the phenomenon of energy transfer in organic nanocrystals. It also allows us to rule out the occurrence of photon-molecule strong coupling and the formation of polaritonic states in these systems.

We can employ Equation (4) to investigate the population dynamics for an initial condition given by  $n_D(t=0) = 1$ ,  $n_A(t=0) = 0$ . By setting  $P = 0$ , we can mimic a lifetime measurement configuration, in which donor molecules are populated by an ultrafast laser pulse. In Figure 3b, we plot the population transients for the donor (continuous) and acceptor (dashed lines) molecules, evaluated at the same densities as in panel (a). The population at the donor molecules decays faster as  $n$  increases, which is again a clear signature of energy transfer to the acceptor chromophores. These become significantly populated within less than 1 ns for  $n \simeq 10^{-4} \text{ nm}^{-3}$ , and  $n_A > n_D$  within a few nanoseconds even for lower values of the acceptor density. These findings also match perfectly with the experimental observations by Chen and co-workers,<sup>[15]</sup> shown as an inset. Here, and for convenience, we plot the experimental multi-exponential fittings to the measured data, rather than the measurements themselves.

To fully characterize the light-harvesting capabilities of the organic nanocrystals, we compute next two physical magnitudes widely employed in the experimental literature:<sup>[11,12]</sup> the energy transfer efficiency and the antenna effect. The former is usually defined as one minus the ratio of the total fluorescence at  $\omega = \omega_D^{em}$  in the absence (presence) of the acceptor ensemble. The latter is given by the ratio of the acceptor contribution to the total fluorescence at  $\omega = \omega_A^{em}$  under only donor and only acceptor pumping conditions. Both magnitudes are shown in Figure 3c as a function of  $n$ . They follow a very similar trend with lower values for the antenna effect at large acceptor concentrations. For  $n = 10^{-4} \text{ nm}^{-3}$ , the energy transfer efficiency reaches 50%, and it amounts to 92% when  $n = 10^{-3} \text{ nm}^{-3}$ . This result is also in excellent agreement with the experimental value (95%).

Finally, we apply our model beyond previous experimental conditions and explore the impact that photon confinement has on the fluorescence spectrum and the energy transfer efficiency in organic nanocrystals. Our results reveal that it is absent in bare structures, and therefore they must be placed



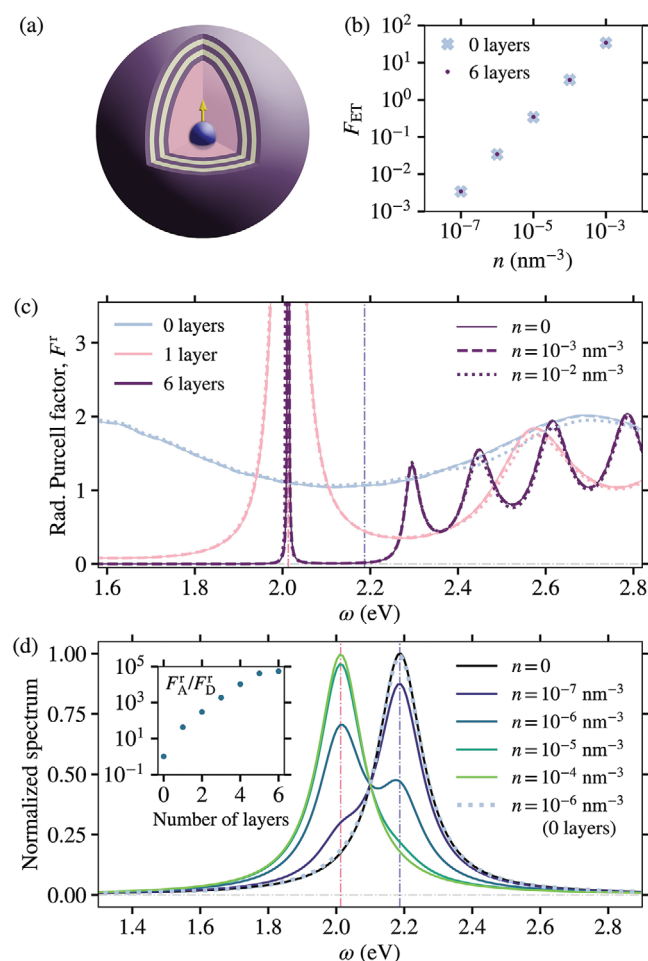


**Figure 4.** a) Sketch of a multilayered optical cavity embedding a spherically-shaped organic nanocrystal. b) Normalized energy transfer rate versus acceptor density for bare (blue crosses) and coated (purple dots) crystals. c) Radiative Purcell spectra for different number of cavity layers and acceptor densities. d) Fluorescence spectrum in six-layered cavities and for low acceptor concentrations. The blue dotted line corresponds to a bare nanocrystal with  $n = 10^{-6} \text{ nm}^{-3}$ , taken as reference. The inset displays the ratio between the radiative Purcell factors evaluated at the donor and acceptor emission frequencies versus the number of cavity layers.

within an optical cavity for this purpose. **Figure 4a** sketches the simple system that we are investigating in the following: a 400 nm radius spherical-shaped crystal is surrounded by a periodic arrangement of 75 nm thick shells of two different materials. These are the donor nanocrystal itself ( $\epsilon = \epsilon_b = 2^{[26]}$ ), and a high refractive index dielectric such as GaP ( $\epsilon = 9^{[35]}$ ). Note that this configuration is not aimed to mimic any experimental sample reported so far. As expected for the Förster mechanism, the optical coating does not have any influence on the donor-acceptor transfer rates. This is clearly shown by **Figure 4b**, which plots  $F_{ET}$  as a function of  $n$ . Gray-blue crosses correspond to the uncoated crystal, and purple dots to its embedding in a cavity comprising six periodic layers, each of them consisting in two shells of different materials. These two sets of results do not only overlap with each other, they also match perfectly the  $F_{ET}$  values in the inset of **Figure 2b**, despite the fact that they were calculated for different structure geometry and dimensions.

Although the optical coating in **Figure 4a** cannot modify the energy transfer rate, it permits tailoring the radiative Purcell spectrum for the system. This is apparent in **Figure 4c**, which plots  $F^r$  versus frequency for cavity-crystal configurations with three different number of layers and acceptor/donor ratios. The cavity has been designed to yield a sharp peak in the radiative Purcell at  $\omega = \omega_A^{\text{em}}$ , and a shallow dip at  $\omega = \omega_D^{\text{em}}$ . We can observe that these two spectral features are sensitive to the number of coating layers but very robust to variations in  $n$ . By simple inspection of Equation (6), we can infer that the radiative enhancement of acceptor molecules and the inhibition of donor ones effectively increases the weight of the acceptor contribution to  $S(\omega)$  at a fixed  $n$ . This is confirmed in **Figure 4d**, which plots the normalized fluorescence spectra of spherical crystals with extremely low acceptor concentrations and surrounded by six-layer cavities. It shows that the emission by the acceptor molecules dominates  $S(\omega)$  at acceptor/donor ratios as small as  $10^{-5}$ , two orders of magnitude lower than in **Figure 3a**. The influence of photon confinement is also clearly illustrated by the comparison of the two fluorescence spectra for  $n = 10^{-6} \text{ nm}^{-3}$ . The cavity transforms the single-peaked donor profile of the bare structure into a doubled-peaked one, in which donor and acceptor contributions have similar weights. The ratio between the radiative Purcell factors for acceptor and donor chromophores in the inset of **Figure 4c** shows the strong dependence of the cavity performance on the number of coating layers. These results show that the fluorescence characteristics of organic nanocrystals can be greatly modified through photon confinement, despite the fact that energy transfer in these systems is completely governed by the Förster mechanism.

### 3. Conclusions

We have presented a theoretical description of energy transfer and fluorescence in organic nanocrystals. It is based on a rate equation treatment of donor and acceptor population dynamics with parameters extracted from electromagnetic simulations. The predictive value and the accuracy of our approach has been demonstrated through a systematic comparison against recent experimental results reporting high transfer efficiencies at extremely low acceptor concentrations. Contrary to a previous explanation of these results, we find that the crystal itself does not provide a significant photon confinement, and therefore no polaritonic effects take place in these systems. In contrast, it is the extremely large donor density which makes Förster transfer so efficient in these nanocrystals. Finally, we propose a cavity-crystal configuration in which the acceptor channel dominates the fluorescence intensity at concentrations orders of magnitude lower than the experimental ones. We believe that our theoretical model is a versatile, insightful and accessible tool that may serve as guidance for the design and characterization of fluorescence emission and energy transfer phenomena in complex artificial photosynthetic structures.

### Acknowledgements

This work was funded by the Spanish Ministry for Science, Innovation, and Universities — AEI grants RTI2018-099737-B-I00, PCI2018-093145 (through

the QuantERA program of the European Commission), and MDM-2014-0377 (through the María de Maeztu program for Units of Excellence in R&D), and by the European Research Council under Grant Agreement ERC-2016-STG-714870. It was also supported by a 2019 Leonardo Grant for Researchers and Cultural Creators, BBVA Foundation.

## Conflict of Interest

The authors declare no conflict of interest.

## Keywords

energy transfer, fluorescence, Förster mechanism, organic nanocrystals, photon confinement

Received: August 24, 2020

Revised: September 20, 2020

Published online: October 21, 2020

- [1] G. D. Scholes, G. R. Fleming, A. Olaya-Castro, R. van Grondelle, *Nat. Chem.* **2011**, 3, 763.
- [2] R. Croce, H. van Amerongen, *Nat. Chem. Biol.* **2014**, 10, 492.
- [3] R. Ziessel, A. Harriman, *Chem. Commun.* **2011**, 47, 611.
- [4] T. Mirkovic, E. Ostroumov, J. M. Anna, R. van Grondelle, Govindjee, G. D. Scholes, *Chem. Rev.* **2017**, 117, 249.
- [5] C. Röger, Y. Miloslavina, D. Brunner, A. R. Holzwarth, F. Würthner, *J. Am. Chem. Soc.* **2008**, 130, 5929.
- [6] X. Zhang, Y. Zheng, T. Yu, J. Chen, G. Yang, Y. Li, *J. Phys. Chem. Lett.* **2014**, 5, 2340.
- [7] M.-S. Choi, T. Yamazaki, I. Yamazaki, T. Aida, *Angew. Chem. Int. Ed.* **2004**, 43, 150.
- [8] E. J. W. List, C. Creely, G. Leising, N. Schulte, A. D. Schlüter, U. Scherf, K. Müllen, W. Graupner, *Chem. Phys. Lett.* **2000**, 325, 132.
- [9] J. Kim, D. T. McQuade, A. Rose, Z. Zhu, T. M. Swager, *J. Am. Chem. Soc.* **2001**, 123, 11488.
- [10] M. Locritani, Y. Yu, G. Bergamini, M. Baroncini, J. K. Molloy, B. A. Korgel, P. Ceroni, *J. Phys. Chem. Lett.* **2014**, 5, 3325.
- [11] D. Zhang, Y. Liu, Y. Fan, C. Yu, Y. Zheng, H. Jin, L. Fu, Y. Zhou, D. Yan, *Adv. Funct. Mater.* **2016**, 26, 7652.
- [12] J. J. Li, Y. Chen, J. Yu, N. Cheng, Y. Liu, *Adv. Mater.* **2017**, 29, 1701905.
- [13] S. Guo, Y. Song, Y. He, X. Y. Hu, L. Wang, *Angew. Chem. Int. Ed.* **2018**, 57, 3163.
- [14] Y. Li, C. Qin, Q. Li, P. Wang, X. Miao, H. Jin, W. Ao, L. Cao, *Adv. Opt. Mater.* **2020**, 8, 1902154.
- [15] P. Z. Chen, Y. X. Weng, L. Y. Niu, Y. Z. Chen, L. Z. Wu, C. H. Tung, Q. Z. Yang, *Angew. Chem. Int. Ed.* **2016**, 55, 2759.
- [16] Y. X. Hu, W. J. Li, P. P. Jia, X. Q. Wang, L. Xu, H. B. Yang, *Adv. Opt. Mater.* **2020**, 8, 2000265.
- [17] D. M. Coles, N. Somaschi, P. Michetti, C. Clark, P. G. Lagoudakis, P. G. Savvidis, D. G. Lidzey, *Nat. Mater.* **2014**, 13, 712.
- [18] X. Zhong, T. Chervy, S. Wang, J. George, A. Thomas, J. A. Hutchison, E. Devaux, C. Genet, T. W. Ebbesen, *Angew. Chem. Int. Ed.* **2016**, 55, 6202.
- [19] X. Zhong, T. Chervy, L. Zhang, A. Thomas, J. George, C. Genet, J. A. Hutchison, T. W. Ebbesen, *Angew. Chem. Int. Ed.* **2017**, 56, 9034.
- [20] M. Du, L. A. Martínez-Martínez, R. F. Ribeiro, Z. Hu, V. M. Menon, J. Yuen-Zhou, *Chem. Sci.* **2018**, 9, 6659.
- [21] F. J. García-Vidal, J. Feist, *Science* **2017**, 357, 1357.
- [22] R. Sáez-Blázquez, J. Feist, A. I. Fernández-Domínguez, F. J. García-Vidal, *Phys. Rev. B* **2018**, 97, 241407.
- [23] D. Coles, L. C. Flatten, T. Sydney, E. Hounsflow, S. K. Saikin, A. Aspuru-Guzik, V. Vedral, J. K.-H. Tang, R. A. Taylor, J. M. Smith, *Small* **2017**, 13, 1701777.
- [24] R. Sáez-Blázquez, J. Feist, E. Romero, A. I. Fernández-Domínguez, F. J. García-Vidal, *J. Phys. Chem. Lett.* **2019**, 10, 4252.
- [25] A. Lishchuk, C. Vasilev, M. P. Johnson, C. N. Hunter, P. Törmä, G. J. Leggett, *Faraday Discuss.* **2019**, 216, 57.
- [26] Y. C. Chen, B. Song, A. J. Leggett, P. Ao, X. Zhu, *Phys. Rev. Lett.* **2019**, 122, 257402.
- [27] T. Förster, *Discuss. Faraday Soc.* **1959**, 27, 7.
- [28] J. R. Lakowicz, *Principles of Fluorescence Spectroscopy*, Springer, New York, **1999**.
- [29] Y. Jiang, Z. Shuai, M. Liu, *J. Phys. Chem. C* **2018**, 122, 18365.
- [30] K. Urano, M. Inoue, *J. Chem. Phys.* **1977**, 66, 791.
- [31] R. Loudon, *The Quantum Theory of Light*, 3rd ed., Oxford University Press, Oxford **2000**.
- [32] P. Z. Chen, H. Zhang, L.-Y. Niu, Y. Zhang, Y.-Z. Chen, H.-B. Fu, Q.-Z. Yang, *Adv. Funct. Mater.* **2017**, 27, 1700332.
- [33] L. Novotny, B. Hecht, *Principles of Nano-Optics*, 2nd ed., Cambridge University Press, Cambridge **2012**.
- [34] M. Ringler, A. Schwemer, M. Wunderlich, A. Nichtl, K. Kürzinger, T. A. Klar, J. Feldmann, *Phys. Rev. Lett.* **2008**, 100, 203002.
- [35] J. Cambiasso, G. Grinblat, Y. Li, A. Rakovich, E. Cortés, S. A. Maier, *Nano Lett.* **2017**, 17, 1219.